# Supplemental Methods

## Mouse tissue collection, staining procedures and image acquisition

For whole-mount staining, tissues were fixed with 4% paraformaldehyde, washed with 10-20% sucrose and 10% glycerol, permeabilized with 0.5% Triton X-100 and blocked with 5% donkey serum. 8-µm deparaffinized tissue sections were subjected to heat-induced epitope retrieval (Low pH Retrieval solution, DAKO). **Supplemental Table 2** describes primary and secondary antibodies. Click-it EdU Alexa Fluor 555 kit (Life Technologies) was used for EdU detection. Images were taken using confocal Zeiss LSM 510 META or Leica SP5 TANDEM microscopes and analyzed using Imaris and Photoshop software. Large image tiles where acquired using a motorized Zeiss time-lapse Axio Observer.Z1 with AxioVision Rel.4.7 software. All images of whole-mount staining are shown in the same orientation, *i.e.* with the direction of flow from the bottom.

## Cell transfection and immunostaining

Cells were fixed with 4% PFA, permeabilized with 0.1% Triton X-100 and blocked with 5% donkey serum. **Supplemental Table 2** describes primary and secondary antibodies. For knockdown experiments, cells were transfected with 66 nM siRNA using Lipofectamine RNAiMAX (Invitrogen). siRNAs are provided in **Supplemental Table 3**. Two different siRNAs or a pool of 4 were used independently to knockdown the gene of interest. Knockdown efficiency was confirmed for each siRNA by RT-qPCR, Western blot analysis, and/or immunostaining (**Figure 3A** and **Supplemental Figure 1A** for *FOXC2*; **Supplemental Figure 2B** for a second *FOXC2* siRNA; **Supplemental Figure 4C** for *YAP1*; **Supplemental Figure 4D** for *TAZ*). Cells were analyzed after 48-72h, or used 24 hours post-transfection for flow experiments.

## In vitro flow experiments

LECs were seeded at confluence on fibronectin-coated slides (µ-Slide $I^{0.8}$ Luer; ibidi), cultured for 24h and subjected to oscillatory (4 dynes/$cm^2$; ¼ Hz, flow changes direction every 4 sec) or laminar flow (4 dynes/$cm^2$) in a parallel plate flow chamber system (ibidi Pump System; ibidi), or kept under static conditions for 48h. At the end of the experiments cells were fixed, stained and mounted using Ibidi Mounting Medium (ibidi GmbH). For EdU incorporation assay, cells were incubated with 1 µg/ml EdU for 24h in the second day of flow.

For time-lapse studies, images were recorded during the second day of flow experiment using a Smart Cytomate unit (Cytomate Technologies BV) or a Zeiss Time-Lapse inverted microscope Axio Observer.Z1, equipped with EC Plan-Neofluar 20x/0.50 Ph2 M27 objective, CTI Controller 3700, Temp Control 37-2 for temperature control, CoolSNAPHQ2 camera, and AxioVison Rel 4.7 software. Movies were reconstructed as sequences of images taken every 15 min for 4-16 hours for Cytomate, or every 5 min for 5 hours for time-lapse microscopy.

## RNA isolation, qPCR and Western blot analyses

RNA was isolated using the Qiagen RNeasy Plus Micro Kit (Qiagen) and reverse transcribed using Transcriptor First Strand cDNA Synthesis Kit (Roche Diagnostics). Alternatively, RNA was amplified using Ovation® Pico WTA System V2 (Nugen). We used StepOnePlus (Applied Biosystems) and SYBR Green PCR Master Mix (Applied Biosystems) for qPCR analyses. Data were analyzed using the comparative Ct (ΔΔCt) method as described by the manufacturer. Supplemental Table 4 provides sequences of PCR primers. Western blotting was performed as described previously (1).

## Quantification

Lymphatic valves identified by high mOrange2 expression were quantified as mature (with visible leaflets) or immature (no visible leaflets) on 4 vessels per mesentery using a Leica M205FA stereomicroscope equipped with DFC300FXR2 camera (Leica) and the LAS AF6000 software. The total number of valves was quantified using tiled images of mesenteries with Photoshop and ImageJ softwares, and normalized to the vessel length using Angiotool (2).

For cell tracing, proliferation and apoptosis analyses, cells were double stained for Prox1 and GFP, Ki67, EdU or activated Caspase3, and at least 5 valves and the downstream lymphangion in a region proximal to the mesenteric lymph node were examined per mesentery.

For in vitro quantifications, images from 10 independent fields per slide and 50-150 cells per image were counted, after exclusion of the image borders. For junction analysis, the total cell surface, VE-cadherin$^+$ cell surface, and the cell perimeter of individual cells was calculated using Photoshop and ImageJ software. Intercellular junctions were classified into linear (thin and continuous), overlapping (thick, with two visible borders) or discontinuous (zigzag-like, with gaps) junctions. The length of each junction type and the total length of gaps per cell were quantified. Junction complexity was calculated as a Minkowski–Bouligand fractal dimension (3) by using Matlab software and the box-counting method, where a value of 1 indicates a regular junction and a value of 2 a highly disorganized junction.

Movies exported as image sequences were analyzed using ImageJ. For Cytomate movies, 200-250 cells were analyzed. Cells detaching from the surface were counted as dying cells, while cells with nuclear division were counted as proliferating cells. Cell motility data and trajectory plots were generated for 50 cells, randomly chosen in 5 fields using manual Tracking and Chemotaxis and Motility plugins (ibidi).

**Supplemental Table 1. GO terms enrichment analysis.**

| GO term ID | Description | P value | Nb genes |
|---|---|---|---|
| **Genes regulated by OSS in a FOXC2-dependent manner** | | | |
| **Down**-regulated (264 genes) | | | |
| GO:0007049 | cell cycle | 2.89E-20 | 65 |
| GO:0000003 | reproduction | 4.46E-02 | 34 |
| GO:0019882 | antigen processing and presentation | 2.03E-02 | 10 |
| GO:0014706 | striated muscle tissue development | 2.03E-02 | 11 |
| GO:0051488 | activation of anaphase-promoting complex activity | 6.02E-03 | 3 |
| GO:0030214 | hyaluronan catabolic process | 2.61E-02 | 3 |
| GO:0043537 | negative regulation of blood vessel endothelial cell migration | 4.22E-02 | 3 |
| **Up**-regulated (188 genes) | | | |
| GO:0036293 | response to decreased oxygen levels | 4.15E-02 | 9 |
| GO:0006695 | cholesterol biosynthetic process | 8.11E-03 | 5 |
| GO:0001974 | blood vessel remodeling | 4.18E-02 | 4 |
| GO:0010862 | positive regulation of pathway-restricted SMAD protein phosphorylation | 1.90E-02 | 4 |
| **Genes regulated by OSS independently of FOXC2** | | | |
| **Down**-regulated (203 genes) | | | |
| GO:0006955 | immune response | 1.92E-04 | 26 |
| GO:0007155 | cell adhesion | 3.57E-02 | 18 |
| GO:0007067 | cell cycle | 3.26E-02 | 11 |
| GO:0055008 | cardiac muscle tissue morphogenesis | 2.16E-02 | 5 |
| **Up**-regulated (102 genes) | | | |
| GO:0006695 | cholesterol biosynthetic process | 2.12E-05 | 6 |
| GO:0034599 | cellular response to oxidative stress | 1.41E-02 | 5 |
| GO:0019322 | pentose biosynthetic process | 2.75E-06 | 4 |
| GO:0030574 | collagen catabolic process | 1.56E-02 | 3 |
| GO:0021636 | trigeminal nerve morphogenesis | 4.79E-03 | 2 |
| **Genes regulated by OSS only upon *FOXC2* knockdown** | | | |
| **Down**-regulated (109 genes) | | | |
| GO:0002253 | activation of immune response | 3.67E-02 | 7 |
| GO:0030335 | positive regulation of cell migration | 3.67E-02 | 7 |
| GO:0048010 | vascular endothelial growth factor receptor signaling pathway | 3.67E-02 | 3 |
| GO:2000110 | negative regulation of macrophage apoptotic process | 2.49E-02 | 2 |

**Supplemental Table 2. Antibodies and dyes.**

| Antigen | Reactivity | Specie | Origin |
|---|---|---|---|
| **Primary antibodies** | | | |
| β-catenin | Human | Rabbit | Millipore (#06-734) |
| Caspase-3 | Human/Mouse | Rabbit | Cell Signaling (#9661) |
| Claudin-5 | Mouse | Rabbit | Life Technologies (#34-1600) |
| Foxc2 | Human/Mouse | Rat | Kind gift from Dr. N. Miura *(Miura et al, 1997, Genomics)* |
| GAPDH | Human | Rabbit | Sigma (#G9545) |
| GFP | - | Rat | BioLegend – Clone FM264G (#338002) |
| Ki67 | Human/Mouse | Mouse | BD Pharmingen – Clone B56 (#556003) |
| Ki67 | Human/Mouse | Rabbit | Abcam (#ab15580) |
| Laminin α5 | Mouse | Rabbit | Kind gift from Dr. L. Sorokin *(Sixt et al, 2001, J Cell Biol)* |
| Lyve-1 | Mouse | Rabbit | AngioBio (11-034) |
| Lyve-1 | Mouse | Rat | R&D – Clone 223322 (#MAB2125) |
| phospho-MLC2 (Thr18/Ser19) | Human | Rabbit | Cell Signaling (#36745) |
| Pecam-1 | Mouse | Rat | BD Pharmingen - Clone MEC 13.3 (#553370) |
| Prox1 | Mouse | Goat | R&D (#F2727) |
| Prox1 | Mouse | Rabbit | AngioBio (#11002) |
| Cy3-conjugated αSMA | Mouse | - | Sigma – Clone 1A4 (#C6198) |
| TAZ | Human/Mouse | Rabbit | Sigma (#HPA 007415) |
| VE-cadherin | Human/Mouse | Goat | R&D (#AF1002) |
| Vinculin | Human | Mouse | Sigma – Clone hVIN-1 (#V9131) |
| YAP1 | Human/Mouse | Rabbit | Cell Signaling (#4912S) |
| YAP1/TAZ | Human | Mouse | Santa Cruz (#sc-101199) |
| ZO-1 | Human | Rabbit | Life Technologies (#402200) |
| **Secondary antibodies** | | | |
| Alexa 488-conjugated | Goat/Mouse Rabbit/Rat | Donkey | Life Technologies |
| Alexa 555-conjugated | Goat/Mouse Rabbit/Rat | Donkey | Life Technologies |

| | | | |
|---|---|---|---|
| Alexa 647-conjugated | Goat/Mouse Rabbit/Rat | Donkey | Life Technologies |
| Alexa 647-conjugated | Rat | Chicken | Life Technologies |
| **Dyes** | | | |
| Click-It Plus EdU Alexa Fluor 555 | - | - | Life Technologies |
| Hoechst 33342 | - | - | Life Technologies |
| Alexa 488-conjugated phalloidin | - | - | Life Technologies (#A12379) |
| DAPI-containing Prolong Gold antifade reagent | - | - | Life Technologies |

**Supplemental Table 3. List of siRNAs.**

| Gene | Species | Company | Reference (sequence) |
|---|---|---|---|
| *Control* | Human | Qiagen | AllStars Neg. Control siRNA -1027281 |
| *FOXC2* | Human | Thermo Scientific (Dharmacon) | FISSH-000119 (AGGUGGUGAUCAAGAGCGAUU)<br>FISSH-000321 (CAACGUGCGGGAGAUGUUCUU) |
| *YAP1* | Human | Thermo Scientific (Dharmacon) | SMARTpool L-012200-00 |
| *TAZ (WWTR1)* | Human | Thermo Scientific (Dharmacon) | SMARTpool L-016083-00 |
| | | Life Technologies (Ambion) | AM16708 – ID 108730 (GGAUUCGAAUGCGCCAAGA) |

**Supplemental Table 4. Real-time qPCR primers.**

| Gene | Species | Forward primer | Reverse primer |
|---|---|---|---|
| *18s* | Human/ Mouse | AGGAATTCCCAGTAAGTGCG | GCCTCACTAAACCATCCAA |
| *mOrange2* | - | GCAGAAGAAGACCATGGGCT | TGATGTCGACGATGTAGGCG |
| *ANKRD1* | Human | AGTAGAGGAACTGGTCACTGG | TGGGCTAGAAGTGTCTTCAGAT |
| *CTGF (CCN2)* | Human | AGGAGTGGGTGTGTGACGA | CCAGGCAGTTGGCTCTAATC |
| *CYR61 (CCN1)* | Human | CCTTGTGGACAGCCAGTGTA | ACTTGGGCCGGTATTTCTTC |
| *Cx37 (GJA4)* | Human | GGTGGGTAAGATCTGGCTGA | GGCCGTGTTACACTCGAAAT |
| *eNOS (NOS3)* | Human | ATGTTTGTCTGCGGCGATGTTAC | ATGCGGCTTGTCACCTCCTG |
| *LYVE-1* | Human | TGGGGATCACCCTTGTGAG | AGCCATAGCTGCAAGTTTCAAA |
| *PECAM-1 (CD31)* | Human | GCTGACCCTTCTGCTCTGTT | TGAGAGGTGGTGCTGACATC |
| *TAZ (WWTR1)* | Human | CAGCCAAATCTCGTGATGAATC | GGTTCTGCTGGCTCAGGGT |
| *VE-cadherin (CDH5)* | Human | GGCAAGATCAAGTCAAGCGTG | ACGTCTCCTGTCTCTGCATCG |
| *YAP1* | Human | ATGGTGGGACTCAAAATCCA | GGTTCGAGGGACACTGTAGC |
| *Ankrd1* | Mouse | AAACGGACGGCACTCCACCG | CGCTGTGCTGAGAAGCTTGTCTCT |
| *Ctgf* | Mouse | GCTTGGCGATTTTAGGTGTC | CAGACTGGAGAAGCAGAGCC |
| *Cyr61* | Mouse | GCCGTGGGCTGCATTCCTCT | GCGGTTCGGTGCCAAAGACAGG |
| *Cx37* | Mouse | GGGCGCTCATGGGTACCTAT | GCTCCATGGTCCAGCCATA |
| *Itga9* | Mouse | TGCTTTCCAGTGTTGACGAGA | TTAAAGGACACGTTGGCATCATA |
| *Prox1* | Mouse | AAGATATGTCCGACATCTCACCTTATTCAG | CACGTCCGAGAAGTAGGTCTTCAG |

## Supplemental Figure 1

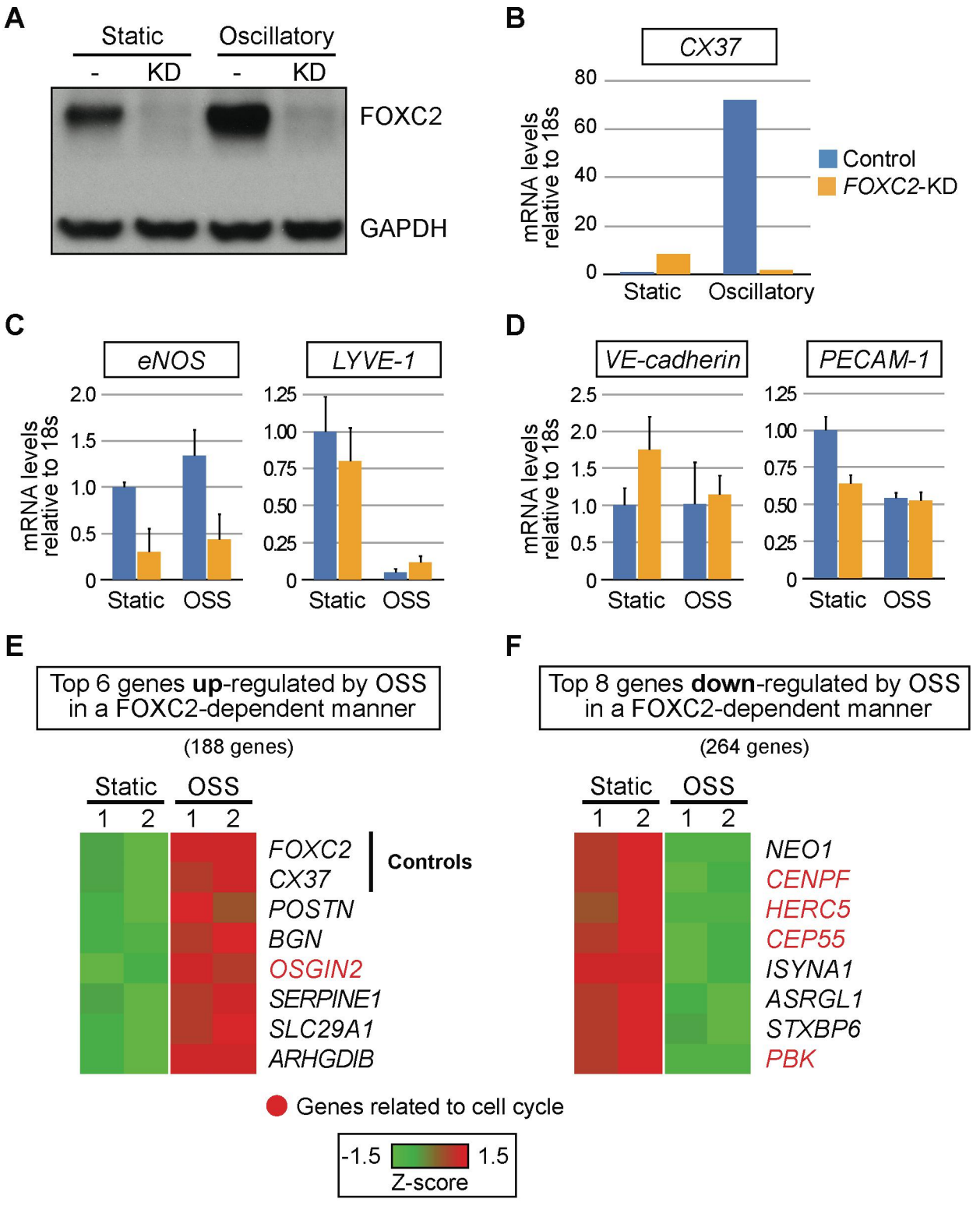


**Supplemental Figure 1. FOXC2 modifies responses of LECs to oscillatory shear stress.**

(**A**) FOXC2 accumulates in cells subjected to OSS, and is absent from cells treated with *FOXC2* siRNAs. Western blot for FOXC2, and GAPDH as a loading control. (**B-D**) Abnormal transcriptional response of *FOXC2*$^{KD}$ cells to shear stress. (**B**) *CX37* is a target of FOXC2 (1, 4). (**C**) *eNOS* is a shear stress-responsive gene, while *LYVE-1* expression is suppressed by shear stress in LECs (1). (**D**) *VE-cadherin* and *PECAM-1* expression are not altered by *FOXC2* knockdown in

cells subjected to OSS. (**E-F**) Heatmaps for the top 6 induced (**E**) or top 8 repressed (**F**) genes by OSS in a FOXC2-dependent manner. Intensity of the heatmap color indicates the Z-score and is proportional to the level of differential gene expression. The total number of genes for each condition is indicated above the heatmap. *FOXC2* and *CX37*, a known target of FOXC2 in LECs under OSS (1) are shown as internal controls. Genes associated with cell cycle by GO term (GO: 0007049) are indicated in red.

## Supplemental Figure 2

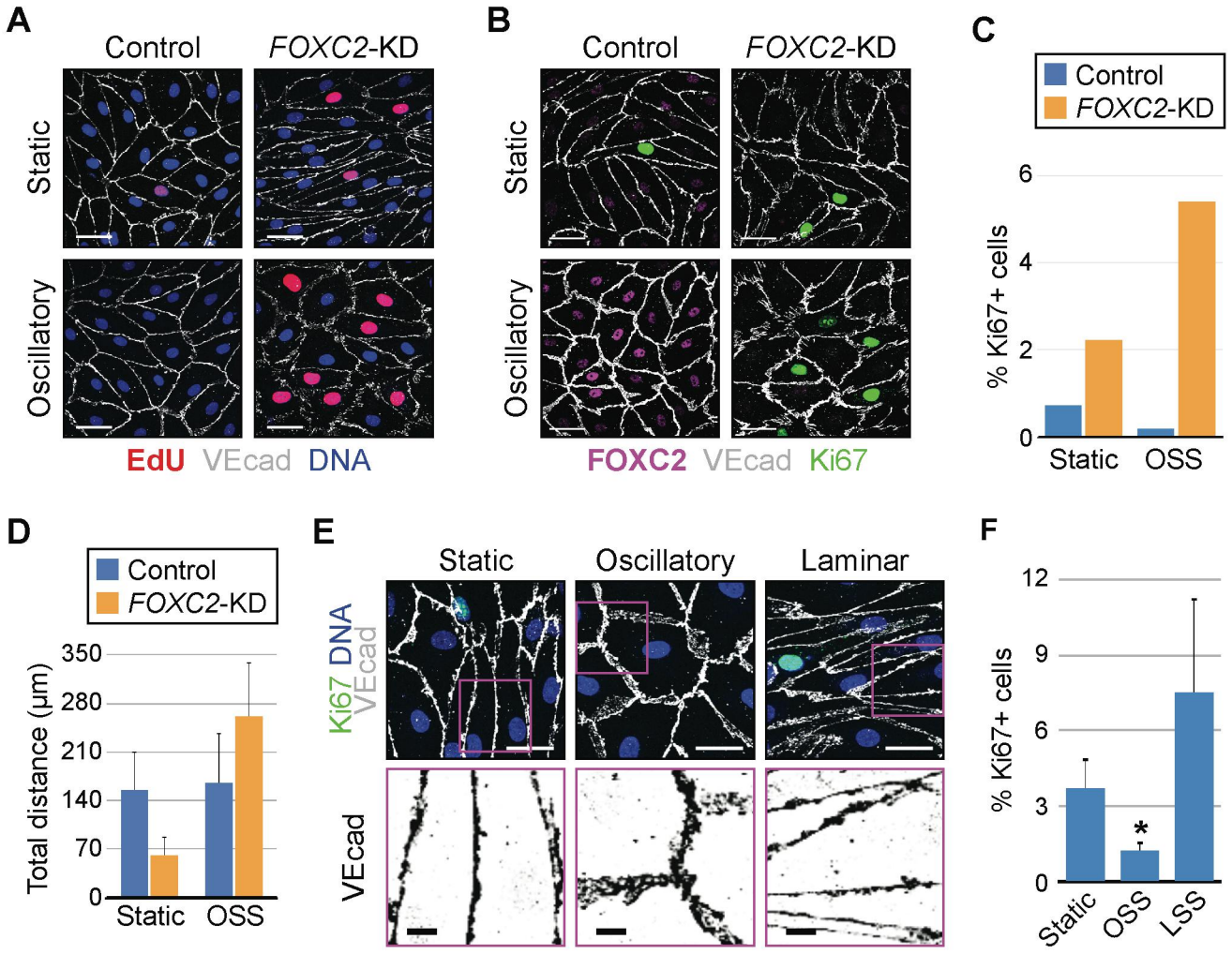


**Supplemental Figure 2. FOXC2 controls the quiescent state of LECs under disturbed flow conditions.**

(**A**) Increased DNA synthesis in *FOXC2*$^{KD}$ cells under OSS conditions. Staining for EdU (red), VE-cadherin (white) and DNA (blue). Scale bar: 10 µm. (**B**) Second *FOXC2* siRNA also induces zigzag junction formation and *FOXC2*$^{KD}$ cell hyperproliferation. Control and *FOXC2*$^{KD}$ cells were stained for FOXC2 (pink), VE-cadherin (white) and Ki67 (green). Scale bar: 10 µm. (**C**) Quantification of Ki67+ cells shown in **B**. (**D**) *FOXC2* knockdown enhances LEC motility under OSS, as indicated by the higher distance covered by cells in 8 hours. $N = 2$. (**E**) OSS, but not LSS, induces overlapping junctions (VE- cadherin, white) and cell quiescence, indicated by the absence of Ki67 staining (green). High-magnification view of the area contained in the pink box is shown below. Scale bars: 20 µm (top) or 5 µm (low). (**F**) OSS, but not LSS, induces LEC quiescence. Quantification of Ki67$^{+}$ cells shown in **E** (n = 3; *, $P < 0.05$).

## Supplemental Figure 3

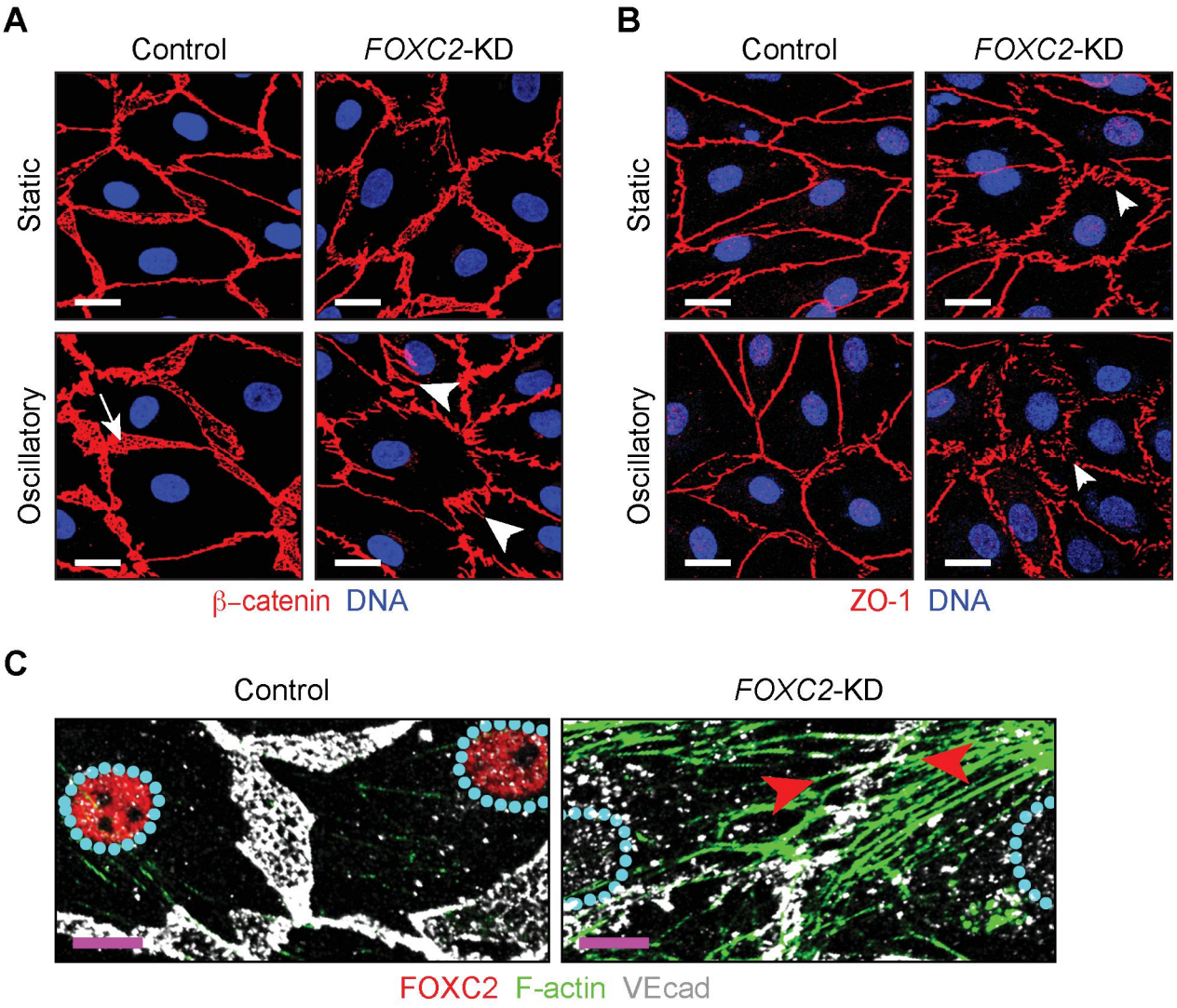


**Supplemental Figure 3. FOXC2 controls cell-cell junction organization.**

(**A**, **B**) Overlapping and zigzag cell-cell junctions in control and *FOXC2*$^{KD}$ cells, as determined by staining for ß-catenin (red in **A**) or ZO-1 (red in **B**). Cell nuclei are stained in blue. (**C**) VE-cadherin (white) is associated with actin stress fibers (green) in *FOXC2*$^{KD}$ zigzag cell-cell junctions. Cells under OSS conditions are shown. Scale bars: 10 µm (**A**, **B**) or 5 µm (**C**).

## Supplemental Figure 4

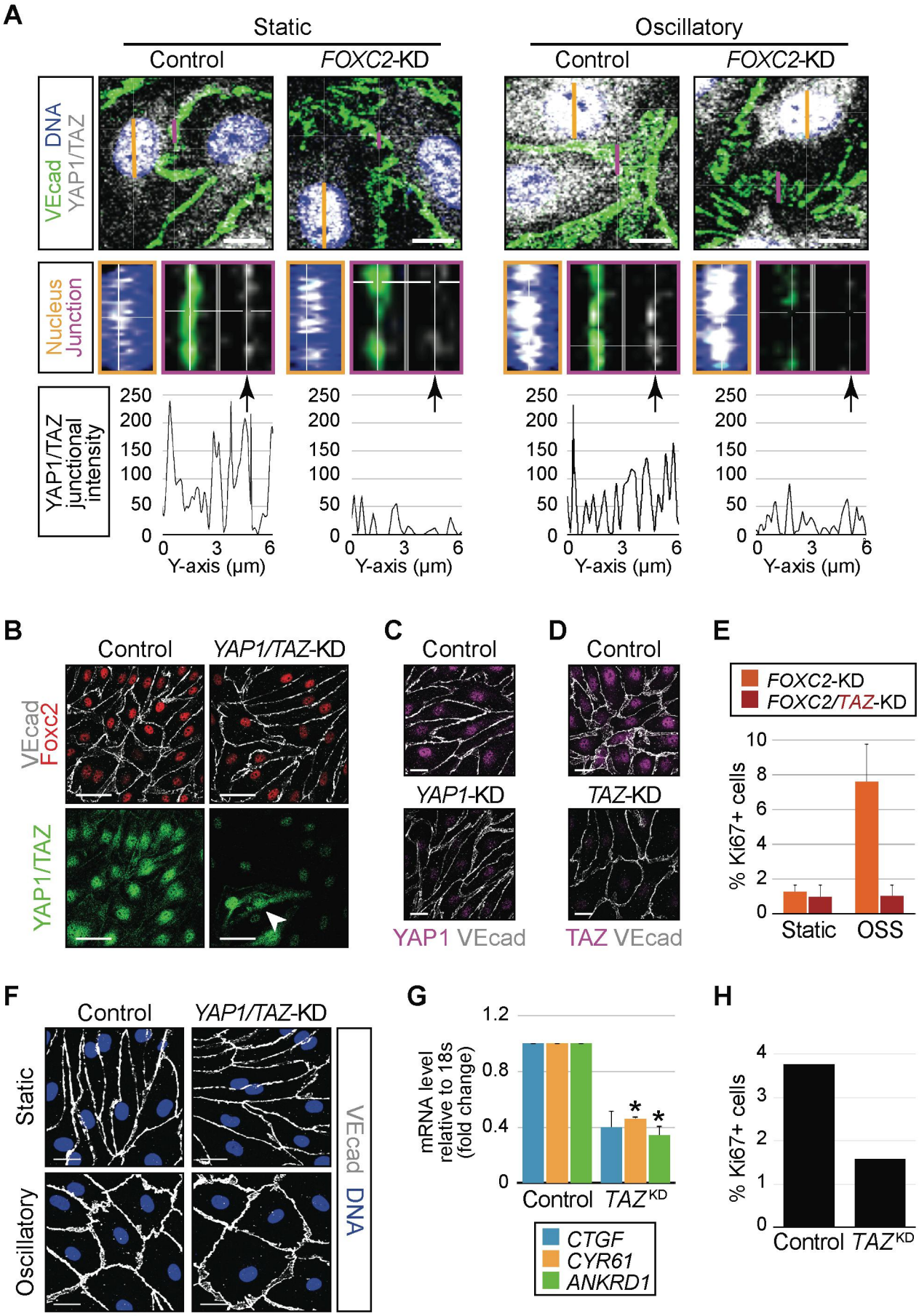

**Supplemental Figure 4. Additional characterization of YAP1/TAZ signaling in *FOXC2*$^{KD}$ cells.**

(**A**) YAP1/TAZ association with the intercellular junctions is FOXC2-dependent. High magnification of control and *FOXC2*$^{KD}$ cell-cell junctions stained for VE-cadherin (green) and YAP1/TAZ (white). DNA is stained in blue. The orange and pink lines indicate localization of the YZ-projection shown below for the nucleus and the junction, respectively. YAP1/TAZ fluorescent intensity profile per junction μm correspond to the area highlighted with the arrow. Scale bar: 5 μm. (**B**) *YAP1/TAZ* knockdown validation. Staining of LECs treated with control or *YAP1+TAZ* siRNAs for VE-cadherin (white), FOXC2 (red) and YAP1/TAZ (green). Arrowhead, cell that was not targeted by siRNAs. Scale bar: 20 μm. (**C, D**) *YAP1* and *TAZ* knockdown validation. Staining for YAP1 (pink, **C**)**,** or TAZ (pink, **D**) and VE-cadherin (white) in LECs transfected with control and *YAP1* in **C**, or *TAZ* in **D** targeting siRNAs. Scale bar: 10 μm. (**E**) Second *TAZ* siRNA also reverses the hyperproliferation of *FOXC2*$^{KD}$ cells. $N = 2$ independent experiments. (**F**) YAP1/TAZ-depletion does not induce VE-cadherin junction remodelling in LECs under static or OSS conditions. Staining for VE-cadherin (white). Scale bar, 10 μm. (**G**) *CTGF* (blue), *CYR61* (orange) and *ANKRD1* (green) gene expression is reduced in LECs treated with TAZ targeting siRNA. $N = 2$; *, $P < 0.05$. (**H**) TAZ knockdown reduces the proportion of Ki67$^{+}$ cells.

## Supplemental Figure 5

**A**

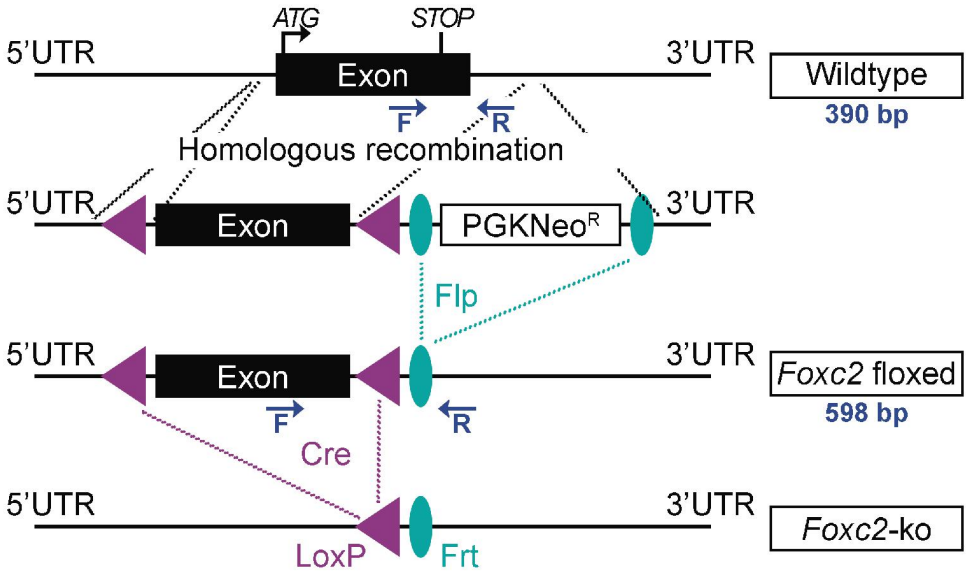


**B**

| Mouse strains | Genetic construct | Reference |
|---|---|---|
| Floxed mice | *Foxc2*$^{lox/lox}$ | Miura N. et al, *unpublished* |
| Inducible Cre deleter | *Prox1*-Cre$^{ERT2}$<br>*Flt4*-Cre$^{ERT2}$ (control) | Bazigou et al, 2011, *J Clin Invest*<br>Stanczuk et al, 2015, *Cell Reports* |
| Lymphatic reporter | *Prox1*-mOrange2 | Haegerling et al, 2011, *Biochem. Soc. Trans* |
| Cre activity reporter | *Rosa26*-YFP | Srinivas et al, 2001, *BMC Dev Biol* |

**C**

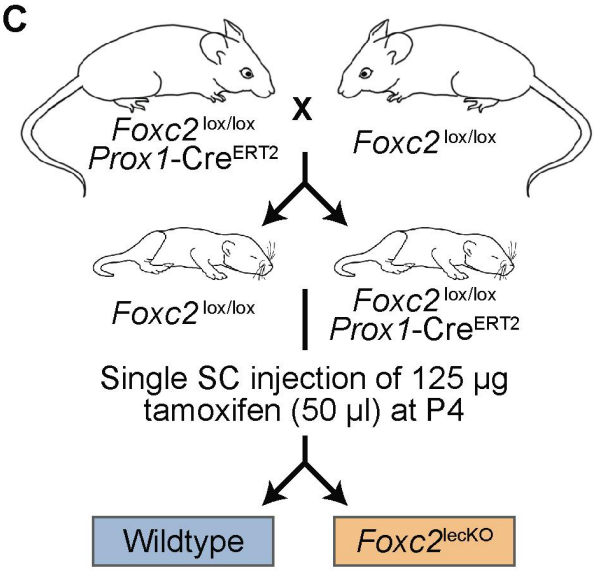


**D**

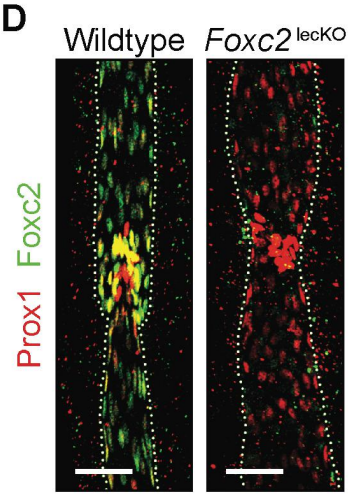


**E**

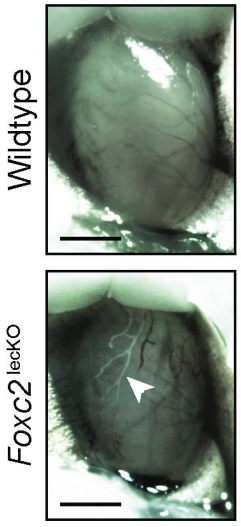


**Supplemental Figure 5. Genetic models used in the study and characterization of *Foxc2*$^{lecKO}$ mouse model.**

**(A)** Targeting strategy for generation of *Foxc2*$^{lox/lox}$ mice. (**B**) Mouse strains used for the analysis (5-8). (**C**) Flowchart of *Foxc2* postnatal deletion and phenotype analysis. (**D**) Efficient deletion of Foxc2 in *Foxc2*$^{lecKO}$ vessels. Staining of P8 mesenteric vessels for Foxc2 (green) and Prox1 (red).

## Supplemental Figure 6

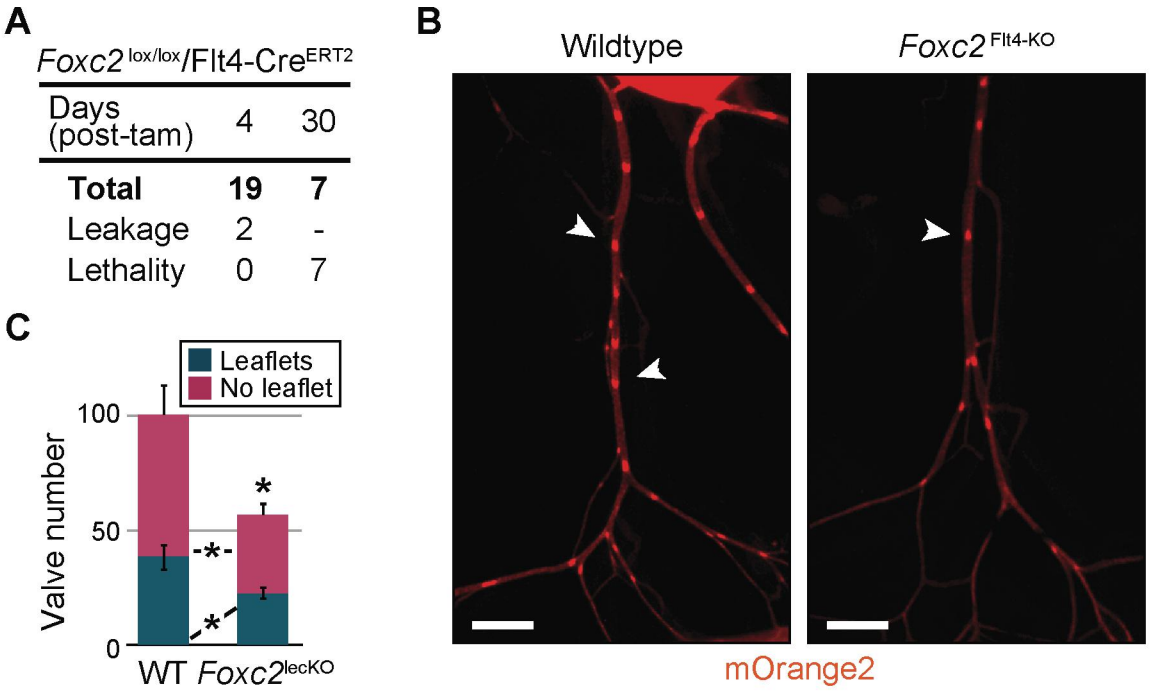


(**E**) Example of chyle backflow into the heart in *Foxc2*$^{lecKO}$ mice. Scale bars: 50 µm (**D**) or 1 mm (**E**).

**Supplemental Figure 6. Postnatal deletion of *Foxc2* induces chyle leakage and lethality.**

(**A**) Inactivation of *Foxc2* using lymphatic endothelial-specific *Flt4*-Cre$^{ERT2}$ deleter strain leads to chyle leakage and lethality. Number of mice analyzed is indicated. (**B**) Mesenteric vessels of *Foxc2*$^{lox/lox}$; *Flt4*-Cre$^{ERT2}$; *Prox1*-mOrange2 mice have reduced number of valves (arrowhead). Scale bars: 500 µm. (**C**) Quantification of the number of valves and their maturation stage in the control and *Foxc2*$^{lox/lox}$; *Flt4*-Cre$^{ERT2}$; *Prox1*-mOrange2 mice . $N = 6$ mice per genotype. * $P < 0.05$.

## Supplemental Figure 7

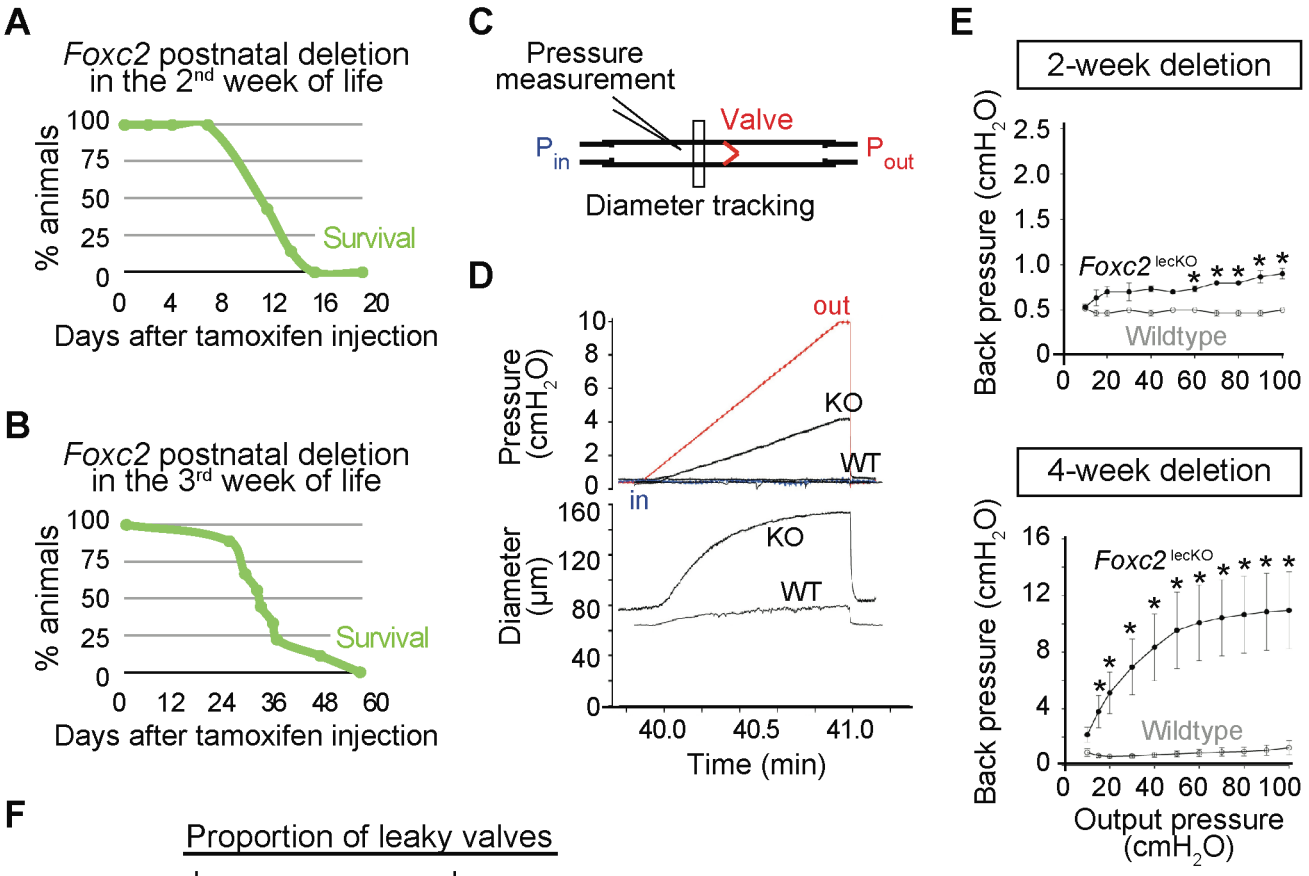


**F**

Proportion of leaky valves

| | **2**-week deletion | | **4**-week deletion | |
|---|---|---|---|---|
| $P_{out}$ | Low | High | Low | High |
| **Wildtype** | 0 / 4 | 0 / 4 | 2 / 12 | 2 / 12 |
| ***Foxc2*** $^{lecKO}$ | 0 / 7 | 3 / 7 | 8 / 16 | 7 / 12 |

**Supplemental Figure 7. *Foxc2* deletion at later time points induces lethality and valve degeneration.**

(**A**, **B**) Survival of mice after *Foxc2* inactivation at P8-P14 (**A**) or P15-P21 (**B**). *N* > 20 per experiment. (**C**) Scheme of the valve back leak experimental setup in adult mesenteric lymphatic collecting vessels. (**D**) Representative recordings of low-pressure tests of valves isolated from the 8-week old wildtype and *Foxc2*$^{lecKO}$ mice treated for 4 weeks with tamoxifen. (**E**) Summary of high-pressure tests of mesenteric valves isolated from mice treated for 2 weeks (upper graph) or 4 weeks (lower graph) with tamoxifen.* $P < 0.05$. See also Figure 9. (**F**) Number of tight and leaky valves in each experimental group presented in **E** and in **Figure 9**, showing impaired function of *Foxc2*$^{lecKO}$ valves.

**Supplemental Figure 8**

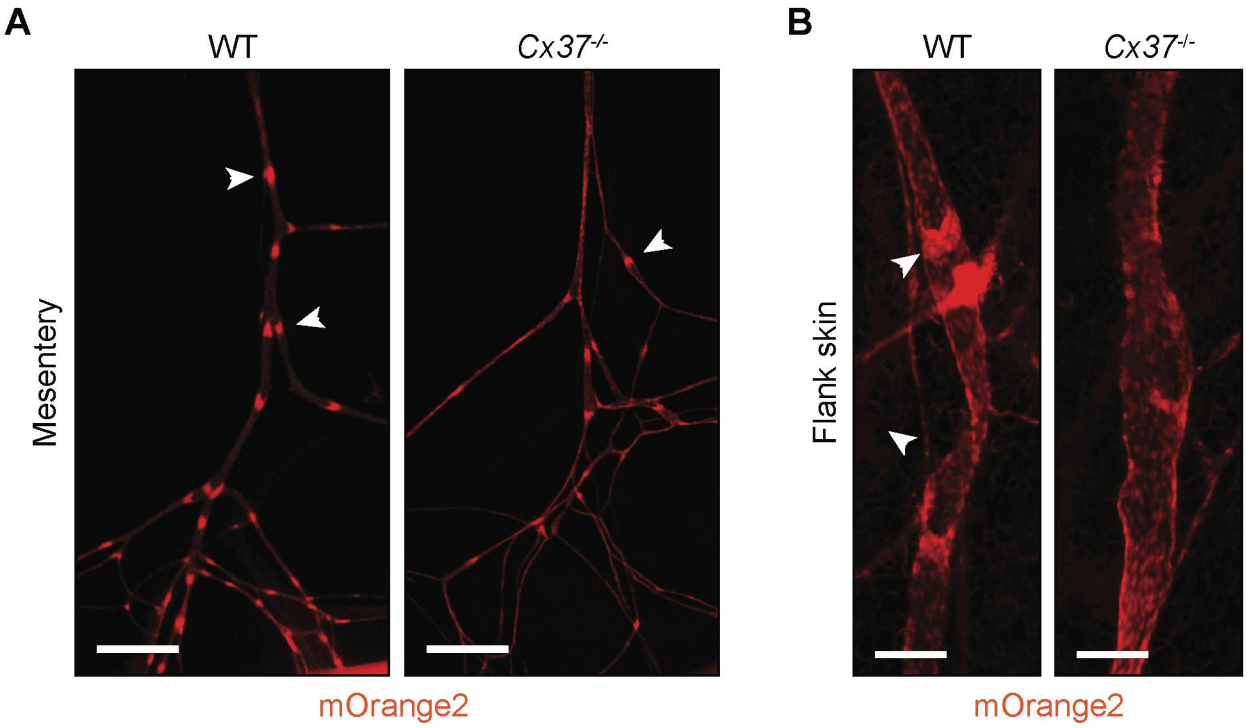


**Supplemental Figure 8. Lymphatic valve paucity, but absence of lymph leakage in Cx37 knockout mouse.**

(**A**, **B**) *Cx37*$^{-/-}$; *Prox1*-mOrange2 mice have reduced number of valves in the mesentery (**A**) and in the skin (**B**), but do not develop macroscopic lymph leakage (0/9 at P8). Scale bars: 500 µm (**A**) or 50 µm (**B**).

## Supplemental Figure 9

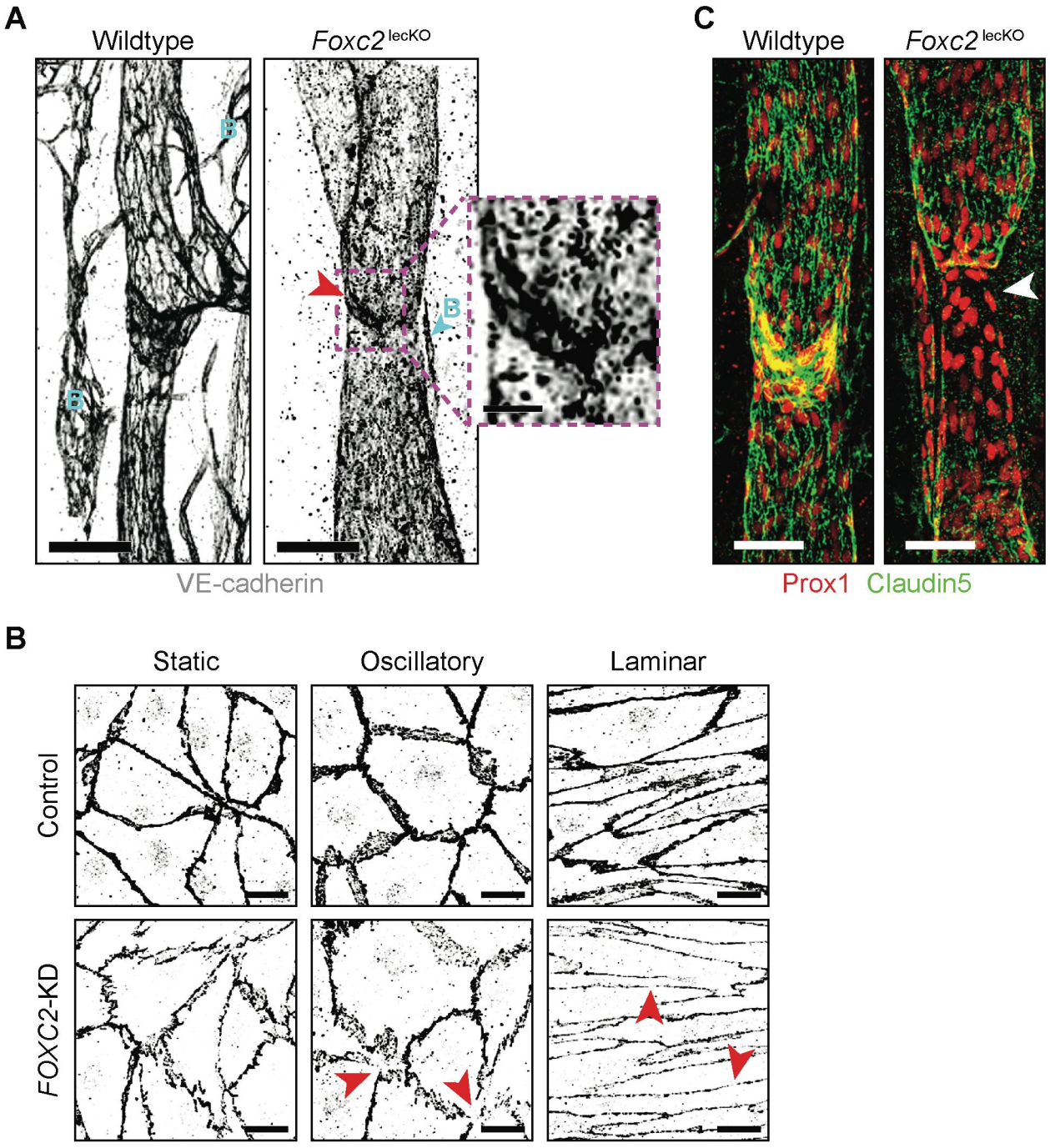


**Supplemental Figure 9. Effects of *Foxc2* inactivation on cell-cell junctions.**

(**A**) VE-cadherin junctions are disrupted in *Foxc2*$^{lecKO}$ P8 mesenteric vessels after 4 days of deletion. B, blood capillary. Red arrowhead, degenerating valve. The dashed pink insert shows a high-magnification view of the degenerating valve. Staining for VE-cadherin (black). Scale bars: 50 µm or 10 µm in the insert. (**B**) *FOXC2* knockdown induces junction disruption and the formation of inter-cellular gaps (red arrowhead), a phenotype potentiated by OSS. Staining for VE-cadherin (black). Scale bars: 10 µm. (**C**) Decreased tight junction protein claudin-5 (arrowhead) in *Foxc2*$^{lecKO}$ P8 mesenteric vessels. Staining for Prox1 (red) and claudin-5 (green). Scale bars: 50 µm.

## Supplemental Figure 10

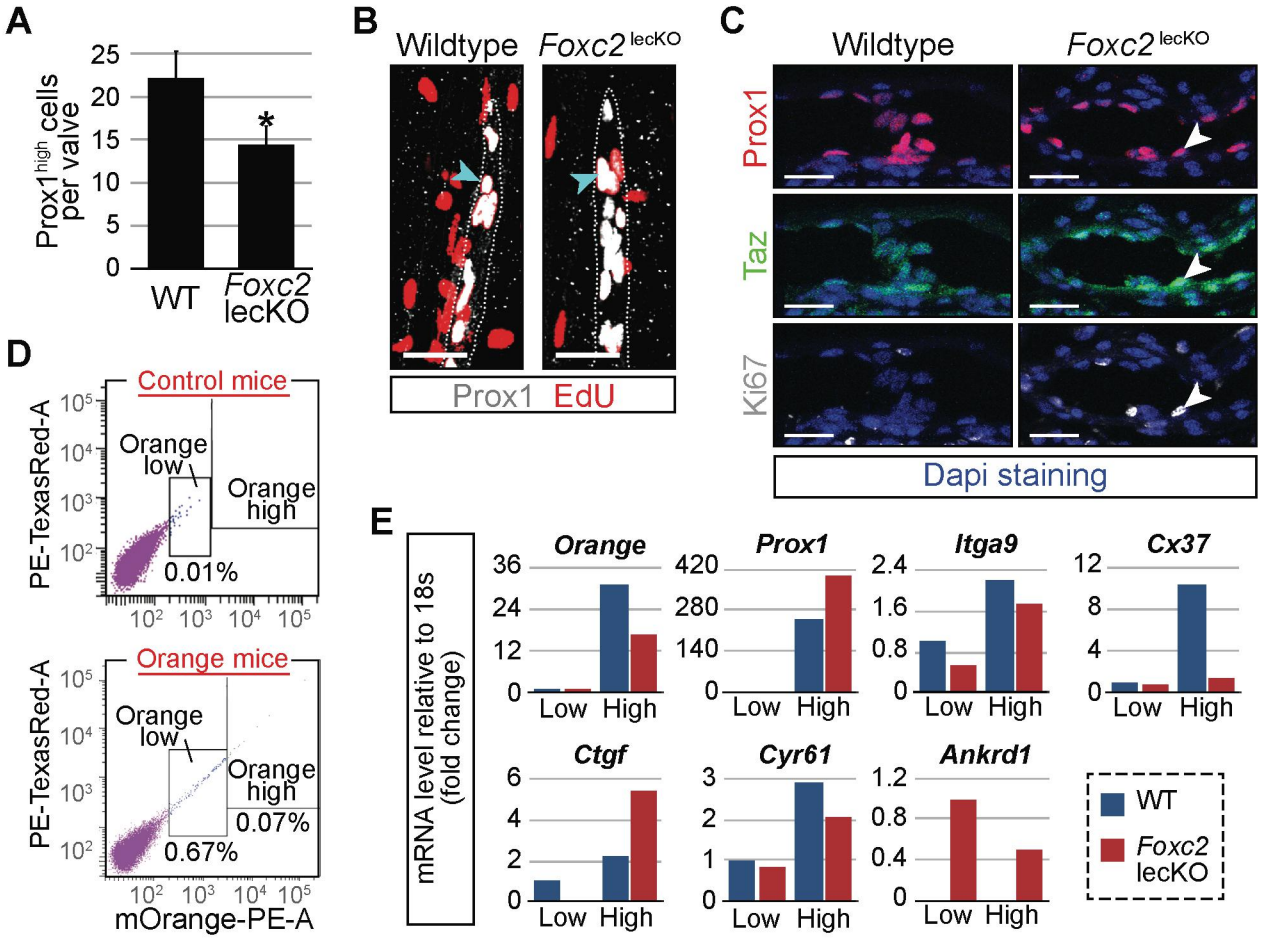


**Supplemental Figure 10. Foxc2 protects valve cells and counteracts Taz signaling.**

(**A**) Reduced number of Prox1$^{HIGH}$ valve cells in *Foxc2*$^{lecKO}$ mice. Mesenteries were collected 2.5 days after tamoxifen injection of P4 animals. The number of Prox1$^{HIGH}$ valve cells was quantified in 3D-reconstructed images (examples are shown in Supplemental Movie 9). WT, $N = 9$; *Foxc2*$^{lecKO}$, $N = 9$. *, $P < 0.005$. (**B**) Wildtype and *Foxc2*$^{lecKO}$ growing mesenteric capillaries have comparable proliferation rates. Capillaries are outlined with a white dashed line. Blue arrowhead, EdU$^{+}$/Prox1$^{+}$ nucleus. Scale bars: 30 µm. (**C**) Mesenteric sections from control and *Foxc2*$^{lecKO}$ mice stained for Prox1 (red), Taz (green) and Ki67 (white), showing nuclear Taz in a Ki67$^{+}$ cell (arrowhead). DNA was stained with DAPI (blue). Scale bars: 20 µm. (**E**) Increased expression of Taz target genes in *Foxc2*$^{lecKO}$ vessels. Analysis by qPCR of control (top panels) and Taz target genes (low panels) in cells sorted by FACS from *Prox1*-mOrange2$^{+}$ wildtype (blue bars, pool of 6 samples) and *Foxc2*$^{lecKO}$ (red bars, pool of 7 samples) mesenteries based on their level of orange fluorescence. **E** is an independent duplicate of the experiment presented in **Figure 13, D-F**.

## Supplemental Figure 11

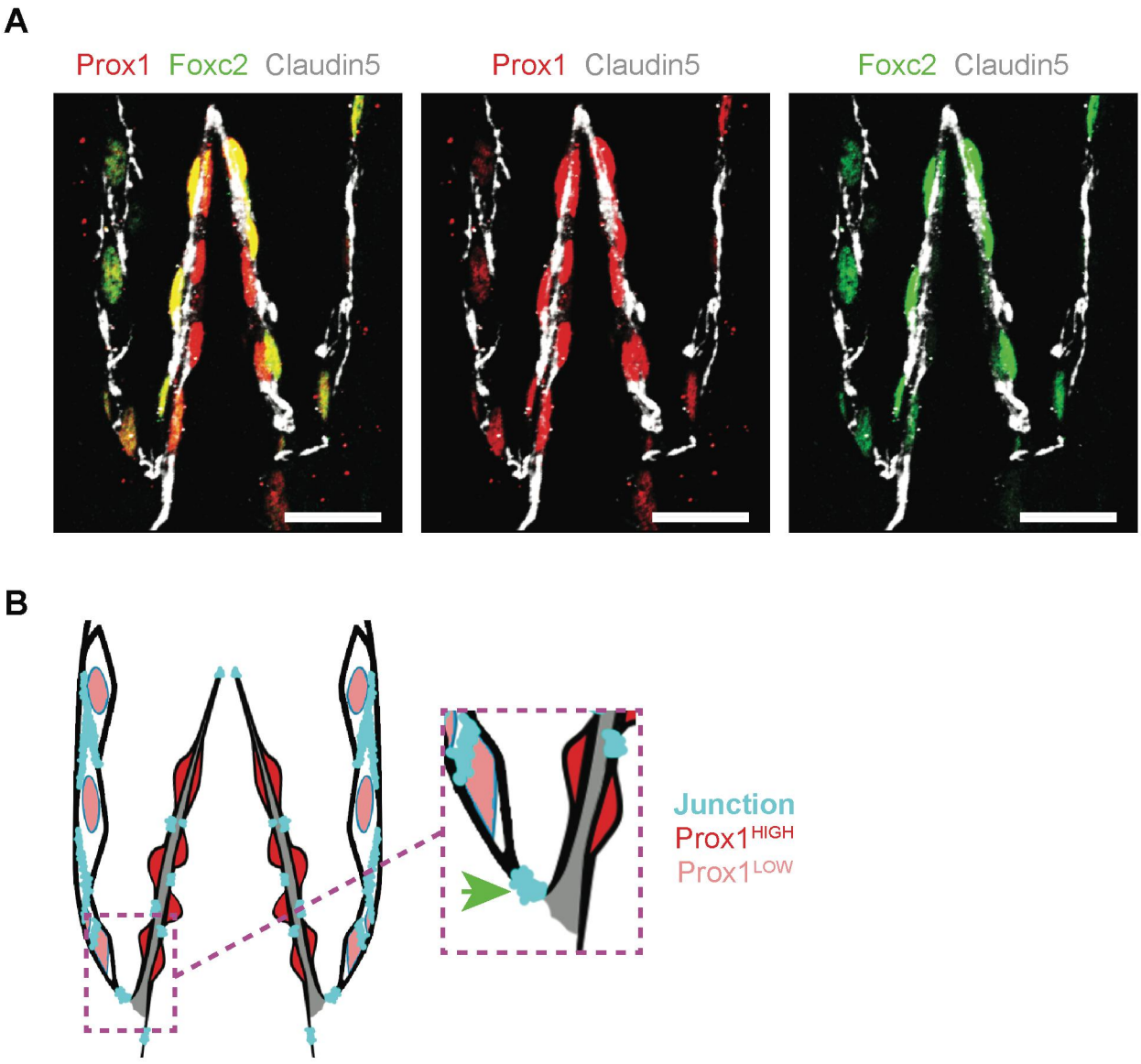


**Supplemental Figure 11. Prox1$^{HIGH}$ cell assembly in the lymphatic valve.**

(**A**) Lymphatic valve leaflet Prox1$^{HIGH}$ cell in direct contact with a lymphangion Prox1$^{LOW}$ cell. Mesenteric valve (7-µm confocal section) stained for Prox1 (red), Foxc2 (green) and Claudin5 (white). Scale bars: 20 µm. (**B**) Recapitulating scheme of Prox1$^{HIGH}$ (red) and Prox1 (low) cell organization within the valve leaflet and sinus, respectively. Intercellular junctions are depicted in blue.

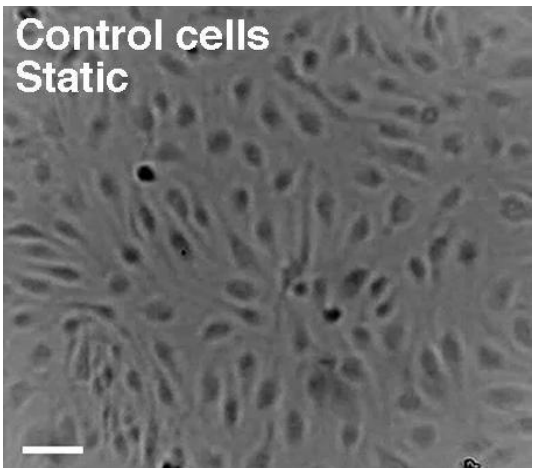


**Supplemental Movie 1. Control cell behavior under static conditions.**

Time-lapse recording of control LECs under static conditions using Cytomate unit. Frames were taken every 15 min for 4 hours; a time stamp is indicated every 1h. Movie was built as 5 frames per second. Pink arrowhead, dying cell; green arrowhead, proliferating cell. Scale bar: 10 μm.

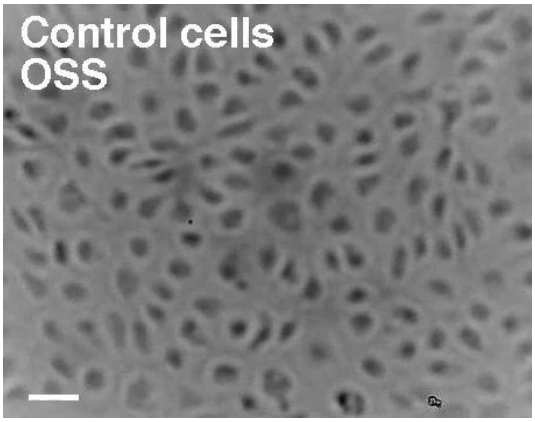


**Supplemental Movie 2. OSS induces control cell quiescence.**

Time-lapse recording of control LECs under oscillatory shear stress conditions using Cytomate unit. Frames were taken every 15 min for 16 hours; a time stamp is indicated every 1h. Movie was built as 5 frames per second. Pink arrowhead, dying cell; green arrowhead, proliferating cell. Scale bar:10 μm.

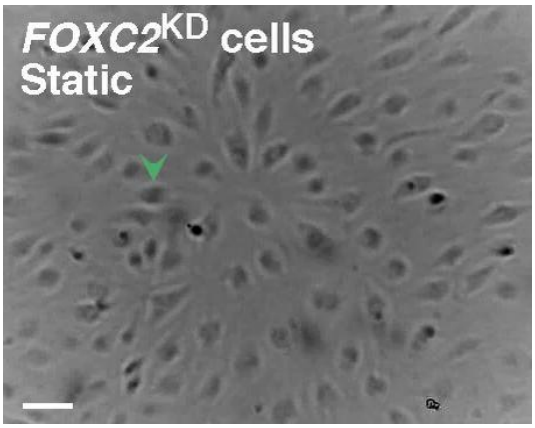


**Supplemental Movie 3. OSS induces *FOXC2*$^{KD}$ cell proliferation and death.**

Time-lapse recording of *FOXC2*$^{KD}$ LECs under static conditions using Cytomate unit. Frames were taken every 15 min for 4 hours; a time stamp is indicated every 1h. Movie was built as 5 frames per second. Pink arrowhead, dying cell; green arrowhead, proliferating cell. Scale bar: 10 μm.

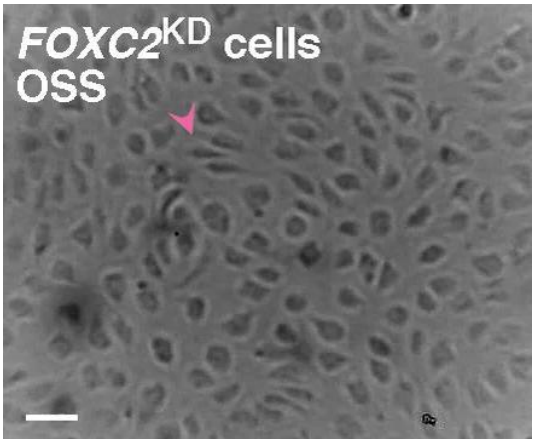


**Supplemental Movie 4. OSS induces *FOXC2*$^{KD}$ cell proliferation and death.**

Time-lapse recording of *FOXC2*$^{KD}$ LECs under oscillatory shear stress conditions using Cytomate unit. Frames were taken every 15 min for 16 hours; a time stamp is indicated every 1h. Movie was built as 5 frames per second. Pink arrowhead, dying cell; green arrowhead, proliferating cell. Scale bar: 10 μm.

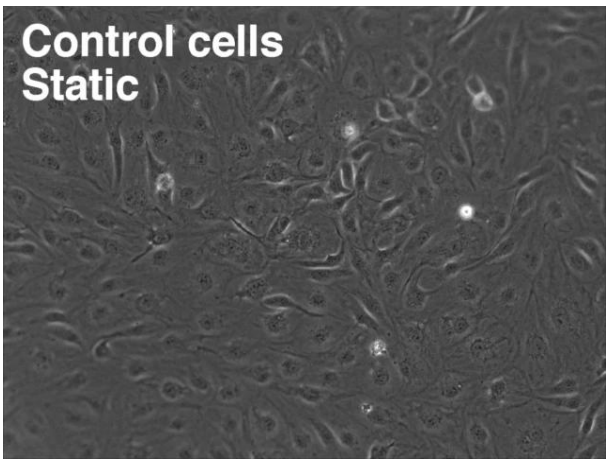


**Supplemental Movie 5. Control cell motility under static conditions.**

Time-lapse microscopy recording of control LECs under static conditions. Frames were taken every 5 min for 5 hours; a time stamp is indicated every 30 min. Movie was built as 3 frames per second.

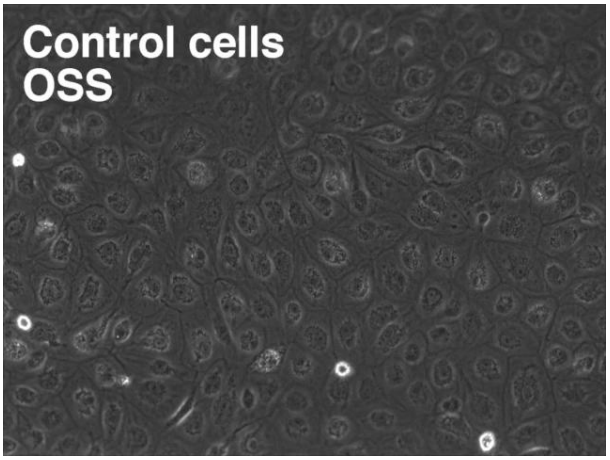


**Supplemental Movie 6. OSS reduces control cell motility.**

Time-lapse microscopy recording of control LECs under oscillatory shear stress conditions. Frames were taken every 5 min for 5 hours; a time stamp is indicated every 30 min. Movie was built as 3 frames per second.

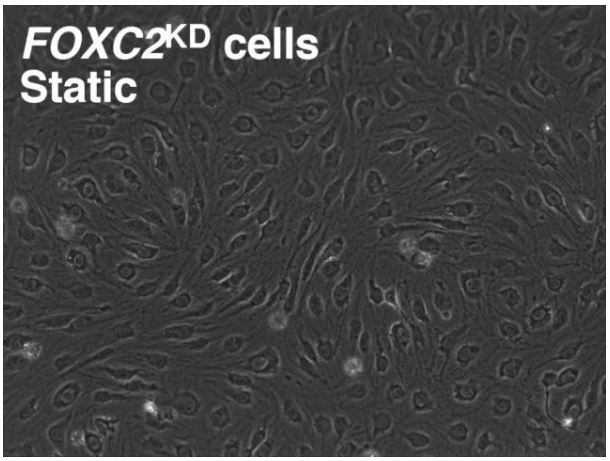


**Supplemental Movie 7. Non-motile *FOXC2*$^{KD}$ cells under static conditions.**

Time-lapse microscopy recording of *FOXC2*$^{KD}$ LECs under static conditions. Frames were taken every 5 min for 5 hours; a time stamp is indicated every 30 min. Movie was built as 3 frames per second.

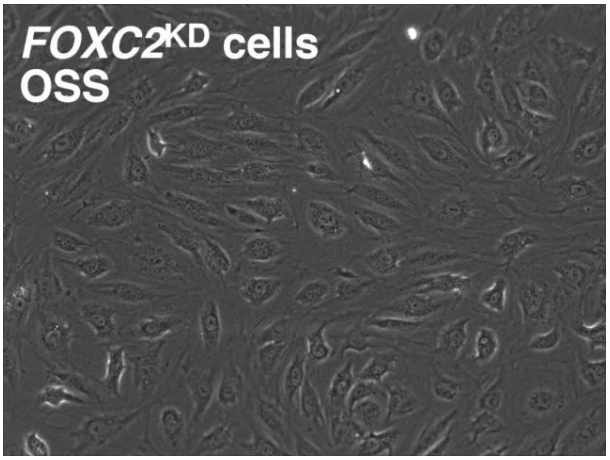


**Supplemental Movie 8. OSS strongly induces *FOXC2*$^{KD}$ cell motility.**

Time-lapse microscopy recording of *FOXC2*$^{KD}$ LECs under oscillatory shear stress conditions. Frames were taken every 5 min for 5 hours; a time stamp is indicated every 30 min. Movie was built as 3 frames per second.

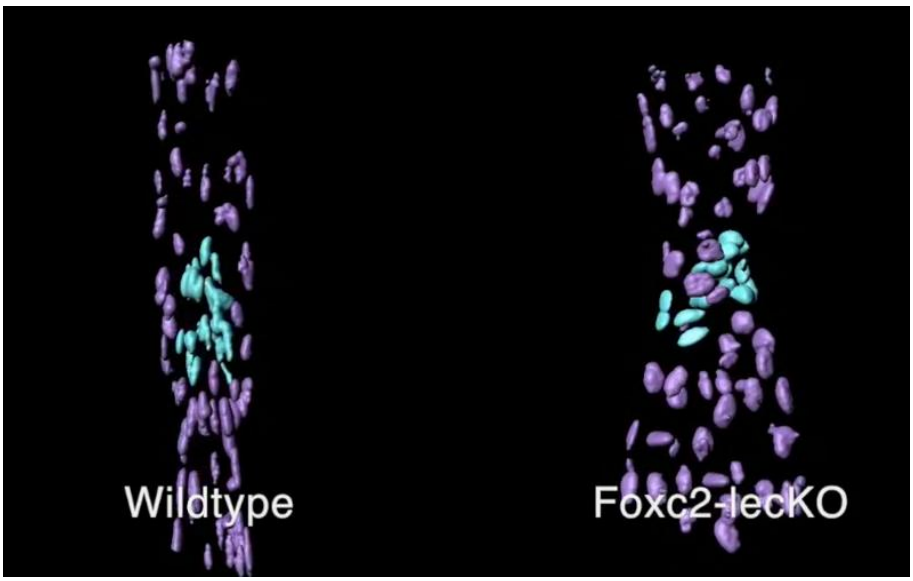


**Supplemental Movie 9. 3D- visualization of wildtype and *Foxc2*$^{lecKO}$ mesenteric lymphatic valves.**

Three-dimensional reconstruction of a mesenteric collecting vessel of a P7 wildtype and *Foxc2*$^{lecKO}$ mouse 3 days after tamoxifen injection, using Imaris “Surpass” function. Valve leaflet cells were pseudo-coloured in blue, while cells forming the vessel wall were pseudo-colored in purple. Note regression of the *Foxc2*$^{lecKO}$ valve area.

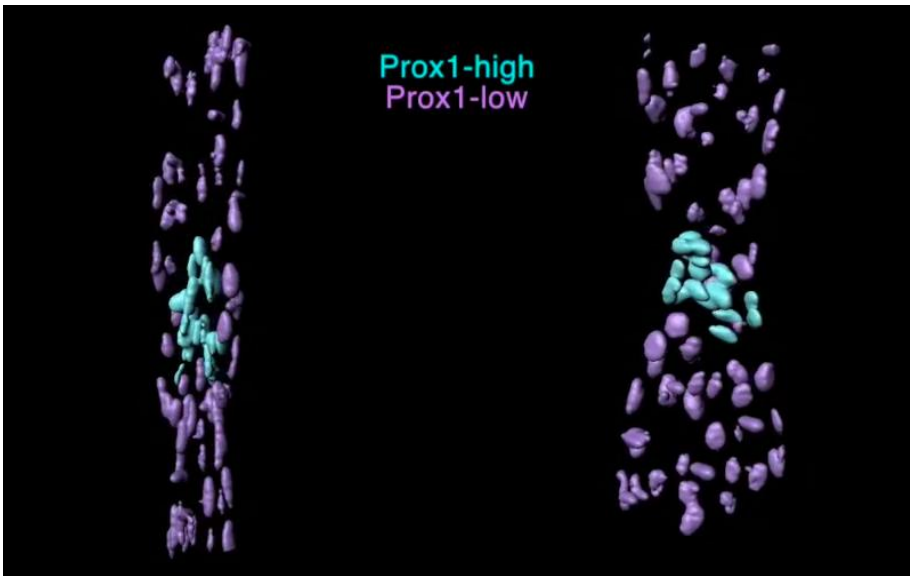

## Supplemental References


1. Sabine A, Agalarov Y, Maby-El Hajjami H, Jaquet M, Hagerling R, Pollmann C, Bebber D, Pfenniger A, Miura N, Dormond O, et al. Mechanotransduction, PROX1, and FOXC2 cooperate to control connexin37 and calcineurin during lymphatic-valve formation. Developmental cell. 2012;22(2):430-45.

2. Zudaire E, Gambardella L, Kurcz C, and Vermeren S. A computational tool for quantitative analysis of vascular networks. PloS one. 2011;6(11):e27385.

3. Kniesel U, Reichenbach A, Risau W, and Wolburg H. Quantification of tight junction complexity by means of fractal analysis. Tissue & cell. 1994;26(6):901-12.

4. Kanady JD, Dellinger MT, Munger SJ, Witte MH, and Simon AM. Connexin37 and Connexin43 deficiencies in mice disrupt lymphatic valve development and result in lymphatic disorders including lymphedema and chylothorax. Developmental biology. 2011;354(2):253-66.

5. Srinivas S, Watanabe T, Lin CS, William CM, Tanabe Y, Jessell TM, and Costantini F. Cre reporter strains produced by targeted insertion of EYFP and ECFP into the ROSA26 locus. BMC developmental biology. 2001;1(4.

6. Bazigou E, Lyons OT, Smith A, Venn GE, Cope C, Brown NA, and Makinen T. Genes regulating lymphangiogenesis control venous valve formation and maintenance in mice. The Journal of clinical investigation. 2011;121(8):2984-92.

7. Hagerling R, Pollmann C, Kremer L, Andresen V, and Kiefer F. Intravital two-photon microscopy of lymphatic vessel development and function using a transgenic Prox1 promoter-directed mOrange2 reporter mouse. Biochemical Society transactions. 2011;39(6):1674-81.

8. Stanczuk L, Martinez-Corral I, Ulvmar MH, Zhang Y, Lavina B, Fruttiger M, Adams RH, Saur D, Betsholtz C, Ortega S, et al. cKit Lineage Hemogenic Endothelium-Derived Cells Contribute to Mesenteric Lymphatic Vessels. Cell reports. 2015.